UC Berkeley
UC Berkeley Previously Published Works

Title

Decoupling Effects of Electrostatic Gating on Electronic Transport and Interfacial Charge-Transfer Kinetics at Few-Layer Molybdenum Disulfide

Permalink

Journal

ISSN

Authors

Maroo, Sonal
Yu, Yun
Taniguchi, Takashi
et al.

Publication Date

DOI

Copyright Information

Peer reviewed

Letter

Decoupling Effects of Electrostatic Gating on Electronic Transport and Interfacial Charge-Transfer Kinetics at Few-Layer Molybdenum Disulfide

Sonal Maroo, Yun Yu, Takashi Taniguchi, Kenji Watanabe, and D. Kwabena Bediako*

Read Online

| ACCESS | Metrics & More | Article Recommendations | SI Supporting Information |

ABSTRACT: The electronic properties of electrode materials play a crucial role in defining their electrochemical behavior in energy conversion and storage devices. The assembly of van der Waals heterostructures and fabrication into mesoscopic devices enable the dependence of an electrochemical response on electronic properties to be systematically interrogated. Here, we evaluate the effect of charge carrier concentration on heterogeneous electron transfer at few-layer MoS_2 electrodes by combining spatially resolved electrochemical measurements with field-effect electrostatic manipulation of band alignment. Steady-state cyclic voltammograms and finite-element simulations reveal a strong modulation of the measured electrochemical response for outer-sphere charge transfer at the electrostatic gate voltage. In addition, spatially resolved voltammetric responses, obtained at a series of locations at the surface of few-layer MoS_2, reveal the governing role of in-plane charge transport on the electrochemical behavior of 2D electrodes, especially under conditions of low carrier densities.

KEYWORDS: SECCM, electrostatic gating, field-effect transistor, 2D MoS_2, electrochemistry
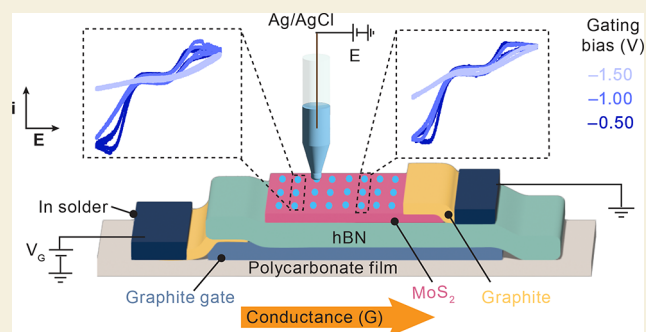
Increasing societal energy demand requires the development of systems that efficiently interconvert electrical and chemical energy.[1] Since electron transfer and electron transport constitute key steps in these interfacial processes,[2,3] a deep understanding of the factors that underpin heterogeneous electron transfer and chemical reactivity is required. Marcus theory[4] provides a powerful framework for understanding homogeneous outer-sphere electron-transfer reactions between two chemical species. Likewise, Gerischer's formulation[5,6] describes the heterogeneous ET rate constant, k_{ET}, in the weak coupling (outer-sphere) limit. For a reduction reaction, k_{ET} is expressed as

$$k_{ET} = \nu_n \int_{-\infty}^{+\infty} \varepsilon(\epsilon) \, f(\epsilon) \, \rho(\epsilon) \, W_{ox}(\lambda, \epsilon) \, d\epsilon$$

where ν_n is the nuclear frequency factor, $\varepsilon(\epsilon)$ is the proportionality function, $f(\epsilon)$ is the Fermi function, $\rho(\epsilon)$ is the density of states of the electrode, $W_{ox}(\lambda, \epsilon)$ is the probability density function of the reactant (oxidized species, ox), and λ is the reorganization energy. Schmickler's theory for electrocatalysis describes how electrochemical reactions in the strong-coupling (inner-sphere) limit, involving the adsorption of an intermediate at the electrode, are also significantly impacted by the structure and dispersion of the electronic bands in the electrode near the Fermi level, ϵ_F.[7] Indeed, several studies have reported the amplification of the interfacial
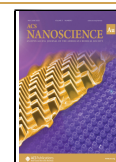
charge-transfer processes caused by defects, edge sites, and grain boundaries on the electrode surface,[8−10] which can be attributed to the localized enhancement in electronic states within their proximity to ϵ_F. These theoretical and experimental studies underscore that interfacial reactivity may be strongly affected by modulating electronic structure. Field-effect transistors (FETs) are the essential components of contemporary electronics, serving as switches and amplifiers in a wide range of applications from smartphones and laptops to sensors and actuators.[11−13] In these devices, an electric field applied via a gate electrode (i.e., electrostatic "gating") is used to modulate the flow of current in the active semiconductor channels. For bulk semiconductors, applying an electric field perturbation alters the alignment of ϵ_F with the conduction/valence bands (and consequently the charge-carrier density) at the semiconductor−dielectric interface but not in the bulk of the material, producing the well-known "band bending" effect.[14] In low-dimensional semiconductors, including two-

dimensional (2D) layers, electrostatic gating controls the band alignments and densities of charge carriers throughout the material.[15−17] 2H-Molybdenum disulfide is a van der Waals (vdW) layered semiconductor with an electronic band gap of 1.29 eV for bulk crystals and 1.8 eV in the monolayer limit.[18−20] Applying an electric field destabilizes the electronic bands with respect to ϵ_F, thereby altering the density of electronic states at ϵ_F as depicted in Figure 1a. The electronic
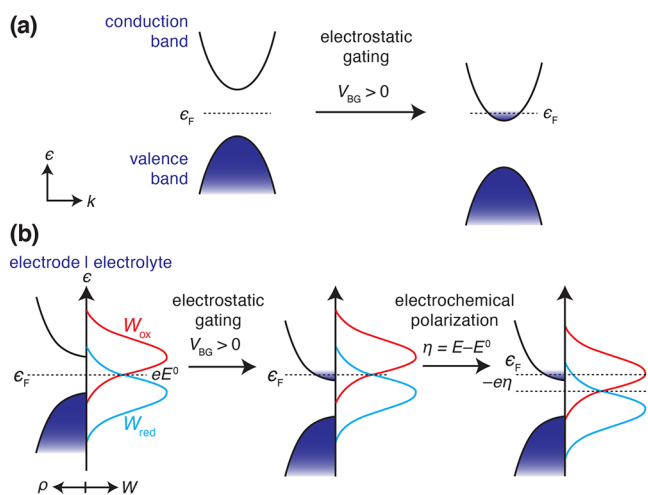
Figure 1. (a) Illustration of the shift in the band edge positions of a semiconducting material relative to ϵ_F upon applying an electrostatic gate voltage, V_{BG}. (b) "Gerischer" schematic illustrating ϵ_F of the semiconducting electrode in relation to the probability distributions of occupied (W_{red}) and empty (W_{ox}) states in solution at equilibrium and after applying an electrostatic gate voltage, V_{BG}, followed by a cathodic overpotential, η.

property manipulation by this FET approach is highly controllable and therefore can provide a powerful means of systematically studying the influence of the density of electronic states on interfacial charge transfer kinetics that may be explained in the framework of the Marcus−Gerischer model; the applied electrostatic gate controls the alignment of the band edges with respect to ϵ_F, and the electrochemical polarization generally controls the alignment of ϵ_F with respect to the solution redox couple (Figure 1b), although we note that the electrochemical polarization can also further gate the semiconductor.[21,22]

Along these lines, previous studies have demonstrated that the heterogeneous charge-transfer kinetics at MoS_2 monolayers can be strongly modulated by applying an external electric field on the working electrodes,[23,24] allowing charge-transfer kinetics at monolayer MoS_2 electrodes to be continuously and reversibly tuned from irreversible to nearly reversible (controlling the standard rate constant over 100-fold) with an applied bottom-gate bias (V_{BG}). Changes in electronic conductivity with electrostatic gating[13,22,25] have also been implicated in affecting the interfacial reactivity. The surface conductance of MoS_2 crystals has been strongly correlated with electrocatalytic activity in electrochemical systems via a "self-gating" effect of the electrochemical polarization itself that produces a highly conductive surface.[22,25] Together, these studies suggest that in an electrochemical system involving semiconducting electrodes, electrostatic gating (whether by the electrolyte itself or a solid-state gate) can affect both intrinsic interfacial electrokinetic behavior (as described formally by the

Marcus−Gerischer equation) and in-plane electronic transport (conductivity), resulting in the net electrochemical response of the system. However, these effects have yet to be deconvoluted in a single set of experiments.

Here we decouple the effects of in-plane charge transport and intrinsic electrokinetics by employing the scanning electrochemical cell microscopy (SECCM) technique[26,27] in an FET configuration. Our FET-SECCM approach enables the acquisition of electrochemical measurements exclusively in select nanoscale regions of the MoS_2 basal plane while keeping the remainder of the flake dry and isolated from concomitant electrostatic gating and conductivity changes by the electrochemical polarization itself; instead, the conductivity of the flake is controlled by the separate electrostatic gate. We obtain spatially resolved voltammetric responses at a series of locations at the surface of few-layer MoS_2 as a function of the gating voltage. Our results reveal the crucial role of in-plane charge transport in governing the electrochemical responses of 2D semiconducting electrodes, especially under conditions of low carrier densities. The experimental approach and results presented here also emphasize the versatility of 2D materials and vdW heterostructures as platforms for probing the physicochemical principles that underpin interfacial electron-transfer reactions.

The atomically thin MoS_2, graphene, and boron nitride (hBN) flakes used in this work were mechanically exfoliated onto SiO_2 (285 nm)/Si substrates from their bulk crystals using the Scotch tape method.[28,29] Flake thicknesses were evaluated using optical contrast (SI Figure 1)[30,31] and atomic force microscopy, AFM (SI Figure 2). The thicknesses of MoS_2 flakes were verified using confocal Raman spectroscopy and photoluminescence spectroscopy (SI Figure 3). Specifically, monolayers of MoS_2 were identified by their strong photoluminescence that arises from a direct band gap in the monolayer limit.[18,32,33] In all electrochemical measurements, the MoS_2 electrodes were fabricated in a field-effect transistor (FET) configuration, as depicted in Figure 2a. Graphite, hBN, and MoS_2 flakes were sequentially stacked over each other by using the vdW dry-transfer method.[34] Further details on sample preparation are provided in the Supporting Information. MoS_2 flakes with thicknesses of one to three layers were assembled on top of an hBN crystal (20−50 nm) as an atomically flat dielectric and a graphite flake as the bottom gate electrode. Figure 2b shows an optical micrograph of a typical vdW heterostructure MoS_2-based FET device used in this work.
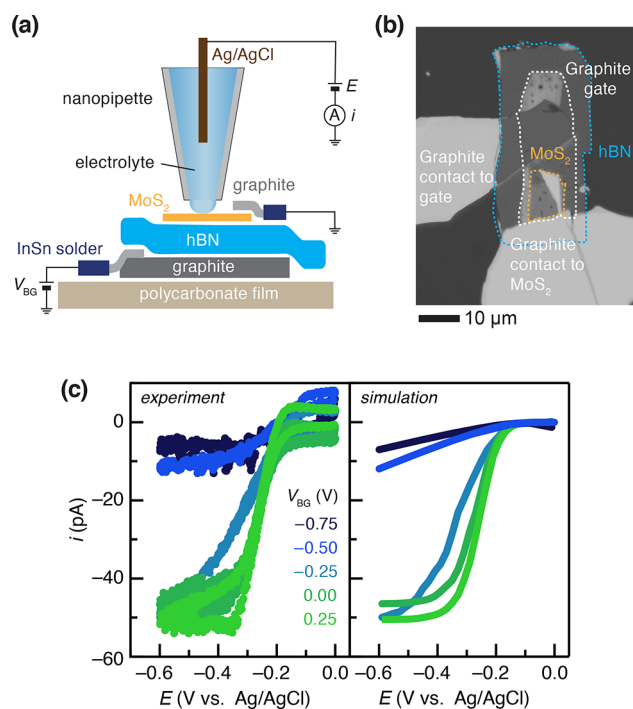
The voltage (V_{BG}) applied to the graphite bottom gate was used to alter the carrier density and exert control over the band alignment. Specifically, the position of ϵ_F shifts either toward or away from the conduction band edge when V_{BG} is modulated as illustrated in Figure 1a. Figure 2c shows the source-to-drain current profile obtained for different V_{BG} values from −0.25 to +2.0 V. The observation of substantial I_{DS} at V_{BG} = 0 V implies that our MoS_2 flakes used in these devices are n-doped possibly due to S vacancies, as is typically the case in transition-metal dichalcogenides.[35] This assertion is further confirmed by the A- and B-exciton peak intensity ratios obtained from the PL spectra (SI Figure 3b). Figure 2c shows that, as expected, the electrical conductance, G, of the MoS_2 layers in these devices ($G = I_{DS}/V_{DS}$) increases with V_{BG}, corresponding to electron accumulation at MoS_2. G saturates at higher V_{BG} as ϵ_F resides well within the conduction band (Figure 2c inset).
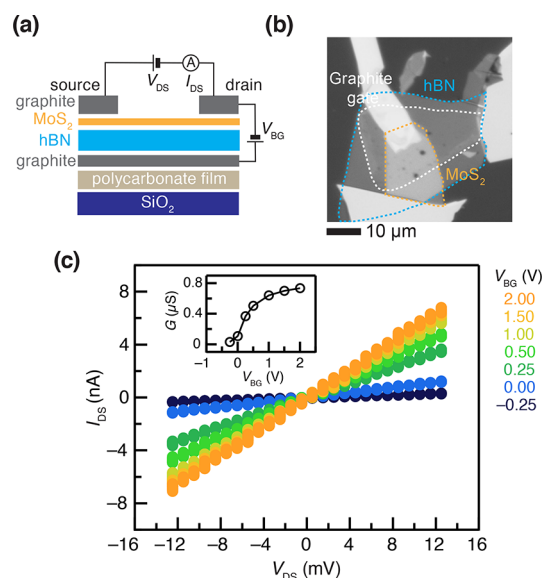
Figure 2. (a) Schematic of the FET device used for electrochemical measurements in this work. V_{DS}: drain–source potential. V_{BG}: bottom-gate voltage. (b) Optical micrograph of a representative bottom-gated monolayer MoS_2 FET device. (c) Two-probe I_{DS} vs V_{DS} curves as a function of V_{BG} at a monolayer MoS_2. The inset shows the two-probe conductance, G, measured as I_{DS}/V_{DS}.

Figure 3. (a) Schematic of a local voltammetric measurement in the SECCM setup. (b) Optical micrograph of a bottom-gated monolayer MoS_2 electrode (hBN thickness: 20 nm). (c) Left: experimental cyclic voltammograms of 1 mM $Ru(NH_3)_6^{3+}$ in 0.1 M KCl solution as a function of V_{BG}. Scan rate: 200 mV/s. Right: simulated voltammograms using parameters in Table 1.

In an electrochemical measurement for such an FET device, we would expect that in addition to tuning the conductance, the position of ϵ_F controlled by V_{BG} would also affect the extent of overlap between filled electronic states of the semiconductor electrode and the probability distribution functions of redox molecules residing in an electrolyte in contact with the semiconductor (Figure 1b). Therefore, in an electrochemical measurement, we would also expect V_{BG} to modulate the intrinsic interfacial electron-transfer kinetics. To probe this effect, we performed SECCM measurements of MoS_2-based devices in the FET configuration. SECCM is a scanning probe technique that enables the interrogation of electron-transfer reactions at the nanoscale using an electrolyte-filled nanopipette that is positioned/scanned over the sample, allowing a micro/nanoelectrochemical cell to be established by contact of the electrolyte meniscus at the base of the pipette and the sample surface.[26,27] As depicted in Figure 3a, we employed quartz nanopipette probes of diameter ~500 nm (SI Figure 4) that were filled with an aqueous electrolyte of 1 mM hexaammineruthenium(III) chloride and 100 mM potassium chloride to make meniscus contact with the gate-tunable MoS_2 surface, creating an enclosed electrochemical cell in which localized voltammetry is performed for a series of V_{BG} values. (See the Supporting Information for additional details of the measurement.) The radii and taper angles of nanopipettes were determined from transmission electron micrographs (SI Figure 4). Figure 3b shows an optical micrograph of a monolayer MoS_2 device measured in this manner, using an hBN flake of 20 nm thickness as the gate dielectric.

Experimental SECCM cyclic voltammograms of Ru-$(NH_3)_6^{3+}$ reduction obtained with nanopipettes probing the center of the gated monolayer MoS_2 flake are shown on the left of Figure 3c. Initially, even at $V_{BG} = 0$ V, the cyclic voltammogram of $Ru(NH_3)_6^{3+}$ exhibits nearly reversible characteristics, which are attributed to the pre-existing n-

doping of MoS_2 discussed above. As V_{BG} is increased to 0.25 V, signifying further electron doping, the reaction shows a measurable enhancement in the apparent interfacial kinetics, displaying a fully electrochemically reversible response, with the plateau (diffusion-limited) current density equaling that of bulk graphite (see SI Figure 5). As V_{BG} is varied from 0.25 to −0.75 V, which involves p-doping (or equivalently, a reduction in n-doping), we observe an anodic shift of the oxidation wave and a decrease in the plateau current in each voltammogram (green to blue). A similar response was observed in the case of the 1 mM ferrocene methanol redox couple (SI Figure 5a). This behavior can be ascribed to an upward shift in the conduction band edge position relative to ϵ_F. This shift of ϵ_F toward the band gap necessarily reduces the charge-carrier concentration, which would substantially impact the electronic density of states available to mediate the interfacial electron transfer as well as the energy state overlap integral between empty (occupied) states of $Ru(NH_3)_6^{3+(2+)}$ and an occupied (empty) state of the same energy in the MoS_2 electrode. These factors would relate to the intrinsic electrokinetic behavior of the material. However, changes in the conductance of MoS_2 should also be expected.

To understand the contributions of intrinsic electrokinetics as well as electronic transport to the electrochemical responses, we used finite-element simulations (COMSOL Multiphysics v.5.6)[36] to model the voltammetric responses and estimate electrochemical rate constants (k^0) and conductance values (G) in our system (SI Figures 6−8). The axisymmetric geometry of the electrochemical cell was modeled with a cylindrical meniscus and a nanopipette, with dimensions determined from TEM images and the limiting current density. The chemical and electron-transfer kinetics of the

redox couples $Ru(NH_3)_6^{+3/+2}$ and $FcMeOH^{3+/2+}$ were modeled using the Nernst−Planck model and Butler−Volmer equations. The in-plane resistance of the electrode was taken into account by modeling it as a resistive film. The initial guesses of G were informed from the measurements described in Figure 2c, after which k^0 and G were then iteratively optimized. The simulated voltammograms were compared to experimental data to refine the simulation parameters. Further details on the finite-element simulation parameters and the procedures for estimating kinetic and transport parameters can be found in the Supporting Information. Table 1 details the

Table 1. Values of G and k^0 for $Ru(NH_3)_6^{+3/+2}$ from the Simulation of CVs at Monolayer MoS$_2$

V_{BG} (V)	$\mathcal{E}$ (mV/nm)	k^0 (cm/s)	G (nS)
0.25	12.5	0.6	≥2.5
0.0	0	0.4	≥2.0
−0.25	−12.5	0.2	0.43
−0.50	−25.0	0.02	0.09
−0.75	−37.5	0.004	0.05

resultant dependence of k^0 and G on V_{BG} for $Ru(NH_3)_6^{+3/+2}$. For comparisons among devices, we also compute and tabulate the electric field $\mathcal{E} = V_{BG}/d_{hBN}$, where d_{hBN} is the thickness of the hBN dielectric used in device fabrication (determined from AFM, SI Figure 2), which typically varies from device to device. These data suggest that the response of the system to electrostatic gating involves the intertwined effects of changing conductivity, and hence conductance, and the intrinsic interfacial kinetics, owing to modulation in electronic densities of states as well as the overlap between the energy states of the reactant and electrode.

These insights notwithstanding, a stronger segregation of the contributions of interfacial kinetics and electronic transport on the electrochemical response required a measurement scheme that provided greater orthogonality in the manipulation of G

and k^0. To gain a deeper understanding of the independent impact of G on the overall electrochemical response, we acquired spatially resolved voltammetric responses by positioning nanopipettes filled with 2.0 mM hexaammineruthenium-(III) chloride, 1.0 mM ferrocene methanol, and 100 mM aqueous potassium chloride at a series of locations at the surface of a bottom-gated trilayer MoS$_2$ electrode (Figure 4a). We note that

$$G = \sigma \frac{A}{L}$$

where σ is the conductivity, L is the length of the channel away from the electrical contact, and A is the cross-sectional area of the channel. We can then define a surface conductivity, σ', as $\sigma' = \sigma A$. Accordingly, for a fixed V_{BG}, σ' would remain constant, yet as we move the pipette from one position to another, G would change as L is varied. Figure 4b shows cyclic voltammograms of ferrocene methanol and hexaammine-ruthenium(III/II) obtained at a series of points at the MoS$_2$ surface with changing distances of 1.4, 9.4, and 16.6 μm from the point of SECCM measurement to the terminal graphite contact.

At $V_{BG} = 0$ V, voltammograms of FcMeOH and $Ru(NH_3)_6^{3+}$ exhibit electrochemically reversible responses at all three locations, consistent with an MoS$_2$ surface that is natively n-doped with sufficient charge carriers to mediate the heterogeneous electron-transfer reactions and also conduct electrical charge without a substantial ohmic drop across the flake. As V_{BG} was varied toward −1.5 V, hole doping via the electric field effect caused pronounced differences in the electrochemical responses at different locations at the MoS$_2$ surface. The voltammogram at location 1, 1.4 μm away from the graphite contact, remained largely unaffected, exhibiting electrochemical reversibility, while the voltammogram at location 3, ∼17 μm away from the graphite contact, displayed a substantial decrease in the Faradaic current associated with both FcMeOH and $Ru(NH_3)_6^{3+}$, producing ostensibly irreversible responses by $V_{BG} = -1.50$ V.
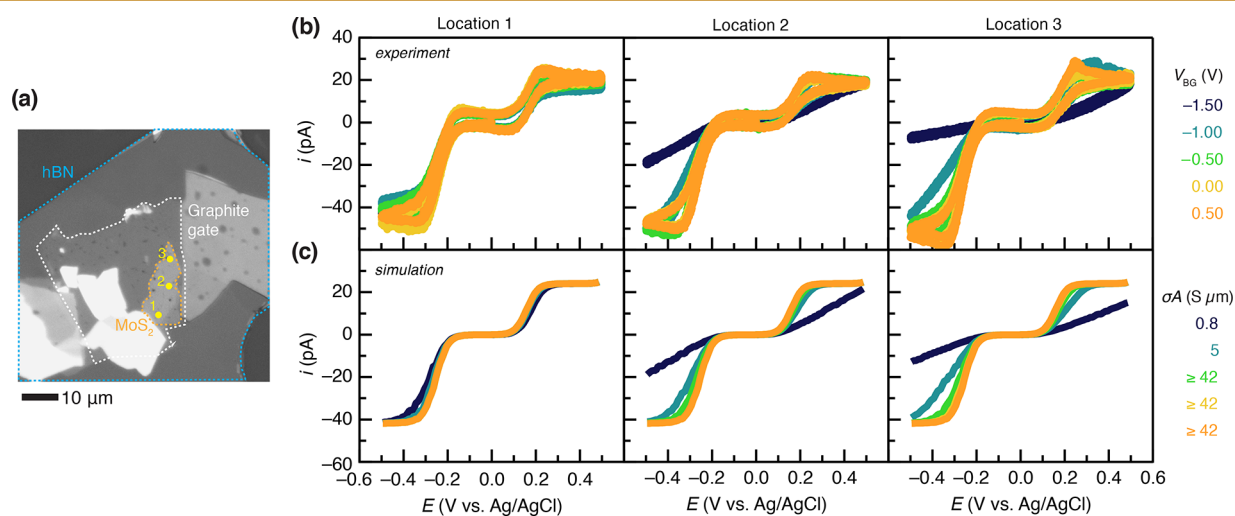
Figure 4. (a) Optical image of a gated three-layer MoS$_2$ electrode using an hBN dielectric of thickness 40 nm. Marked spots 1−3 represent the locations probed by SECCM, varying the distance, L, from measurement to the graphite electric contact. (b) Cyclic voltammograms of 1 mM FcMeOH and 2 mM $Ru(NH_3)_6^{3+}$ in 0.1 M KCl solution as a function of V_{BG} at locations 1 (left), 2 (middle), and 3 (right). Scan rate = 200 mV/s. (c) Simulated cyclic voltammograms (scan rate = 200 mV/s) using the values of k^0 and G are detailed in Table 2. The effects of V_{BG} are incorporated via a changing surface conductivity, $\sigma' = \sigma A$.

Table 2. Location-Dependent Values of G and k^0 for Electrochemical Responses of FcMeOH and $Ru(NH_3)_6^{3+/2+}$ at Trilayer MoS_2

V_{BG} (V)	$\mathcal{E}$ (mV/nm)	k^0 (cm/s)	G (nS) at $L = 1.4\ \mu m$	G (nS) at $L = 9.4\ \mu m$	G (nS) at $L = 17\ \mu m$
0.5	12.5	≥0.1	≥2.5	≥2.5	≥2.5
0	0	≥0.1	≥2.5	≥2.5	≥2.5
−0.5	−12.5	≥0.1	≥2.5	≥2.5	≥2.5
−1.0	−25.0	0.085 ± 0.005	≥2.5	0.55 ± 0.06	0.290 ± 0.003
−1.5	−37.5	0.055 ± 0.002	≥2.5	0.083 ± 0.003	0.047 ± 0.004

The set of measurements displayed in Figure 4b provides a means of systematically probing the effects of electrostatic gating on conductivity and intrinsic charge-transfer kinetics by iterative comparison with finite-element simulations. In simulations, the effect of electrostatic gating was incorporated through a V_{BG}-dependent but location-independent set of k^0 and σ' values while further considering changes to the in-plane electronic transport via a location-dependent (inversely proportional to L) set of G values at each site. CV simulations within this framework (SI Figures 8 and 9) are instructive, revealing that at low conductance levels ($G \leq 0.05$ nS) increasing k^0 even by 2 orders of magnitude does not substantially influence the current profile. Instead, G overwhelmingly governs the rate of interfacial electron transfer in this regime. However, as G increases, both G and k^0 contribute substantially to the overall electrochemical behavior. SI Figures 8 and 9 show that ultimately for $G \geq 0.5$ nS increasing G further does not influence the current profile and k^0 solely determines the overall interfacial electron-transfer rate.

Against this backdrop, we iteratively optimized k^0 and G to reproduce the experimental data in Figure 4b. The simulation parameters that were found to most closely replicate the experimental data are detailed in Table 2, and the simulated voltammograms are presented in Figure 4c. We find good replication of the redox behavior for both FcMeOH and $Ru(NH_3)_6^{3+/2+}$ using effectively identical k^0 values, which are the singular k^0 values presented in Table 2. We note that for the reasons described above, in some locations and at some values of V_{BG}, we can rigorously provide only lower-limit values of k^0 and/or G. Nevertheless, these results provide an instructive illustration of the interplay between in-plane charge transport and intrinsic interfacial electrokinetics.

In conclusion, electrostatic gating of semiconducting electrodes results in the modulation of intrinsic electrochemical kinetics as well as the electronic transport properties. The FET scheme provides an orthogonal knob to control interfacial charge transfer, distinct from the applied electrochemical bias, but the effects of in-plane transport must be considered. This work demonstrates that vdW heterostructures of few-layer MoS_2, graphite, and hBN provide a distinctive platform for interrogating charge-transfer kinetics and electronic transport effects when coupled with SECCM. SECCM enables the exclusion of electrochemical gating effects on in-plane transport, allowing electronic transport to be controlled exclusively by the solid-state gate. Combined experimental measurements and finite-element simulations show how in-plane charge transport has a pronounced effect on the apparent electron-transfer kinetics at semiconducting electrodes, especially at lower charge-carrier densities.

■ ASSOCIATED CONTENT

ⓈⒾ Supporting Information

The Supporting Information is available free of charge at https://pubs.acs.org/doi/10.1021/acsnanoscienceau.2c00064.

General methods, additional experimental data, and finite element simulations (PDF)

■ AUTHOR INFORMATION

Corresponding Author

D. Kwabena Bediako − *Department of Chemistry, University of California, Berkeley, California 94720, United States; Chemical Sciences Division, Lawrence Berkeley National Laboratory, Berkeley, California 94720, United States;* ⓞ orcid.org/0000-0003-0064-9814; Email: bediako@berkeley.edu

Authors

Sonal Maroo − *Department of Chemistry, University of California, Berkeley, California 94720, United States*

Yun Yu − *Department of Chemistry, University of California, Berkeley, California 94720, United States; Present Address: Department of Chemistry, George Mason University, Fairfax, Virginia 22030, United States;* ⓞ orcid.org/0000-0002-0204-1012

Takashi Taniguchi − *International Center for Materials Nanoarchitectonics, National Institute for Materials Science, Tsukuba 305-0044, Japan;* ⓞ orcid.org/0000-0002-1467-3105

Kenji Watanabe − *Research Center for Functional Materials, National Institute for Materials Science, Tsukuba 305-0044, Japan;* ⓞ orcid.org/0000-0003-3701-8119

Complete contact information is available at:
https://pubs.acs.org/10.1021/acsnanoscienceau.2c00064

Author Contributions

CRediT: **Sonal Maroo** conceptualization (equal), data curation (lead), formal analysis (equal), writing-original draft (equal), writing-review & editing (equal); **Yun Yu** conceptualization (equal), data curation (equal), writing-review & editing (equal); **Takashi Taniguchi** resources (equal); **Kenji Watanabe** resources (equal); **D. Kwabena Bediako** conceptualization (equal), funding acquisition (lead), project administration (lead), writing-review & editing (equal).

Notes

The authors declare no competing financial interest.

ACKNOWLEDGMENTS

REFERENCES

(1) Ding, Q. *The Chemistry of MoS₂ and Related Compounds and Their Applications in Electrocatalysis and Photoelectrochemistry.* Ph.D. Thesis, University of Wisconsin—Madison, 2016.

(2) Cannon, R. D. *Electron Transfer Reactions*; Butterworth-Heinemann: 1980; pp 3−95.

(3) Seh, Z. W.; Kibsgaard, J.; Dickens, C. F.; Chorkendorff, I.; Nørskov, J. K.; Jaramillo, T. F. Combining theory and experiment in electrocatalysis: Insights into materials design. *Science* **2017**, *355*, 4998.

(4) Marcus, R. A. Electron transfer reactions in chemistry. Theory and experiment. *Rev. Mod. Phys.* **1993**, *65*, 599−610.

(5) Gerischer, H. Über den ablauf von redoxreaktionen an metallen und an halbleitern: I. Allgemeines zum elektronenübergang zwischen einem festkörper und einem redoxelektrolyten. *Z. Phys. Chem.* **1960**, *26*, 223−247.

(6) Gerischer, H. Über den ablauf von redoxreaktionen an metallen und an halbleitern: III. Halbleiterelektroden. *Z. Phys. Chem.* **1961**, *27*, 48−79.

(7) Schmickler, W.; Santos, E. *Interfacial Electrochemistry*; Springer: Berlin, 2010; pp 145−206.

(8) Li, H.; Tsai, C.; Koh, A. L.; Cai, L.; Contryman, A. W.; Fragapane, A. H.; Zhao, J.; Han, H. S.; Manoharan, H. C.; Abild-Pedersen, F.; Nørskov, J. K.; Zheng, X. Activating and optimizing *MoS₂* basal planes for hydrogen evolution through the formation of strained sulphur vacancies. *Nature Mat* **2016**, *15*, 48−53.

(9) Bentley, C. L.; Kang, M.; Unwin, P. R. Nanoscale Structure Dynamics within Electrocatalytic Materials. *J. Am. Chem. Soc.* **2017**, *139*, 16813−16821.

(10) Mariano, R. G.; Mckelvey, K.; White, H. S.; Kanan, M. W. Selective increase in CO2 electroreduction activity at grain-boundary surface terminations. *Science* **2017**, *358*, 1187−1192.

(11) Moskowitz, S. L. *Advanced Materials Innovation: Managing Global Technology in the 21st century*; Wiley: 2016; pp 152−233.

(12) *Comprehensive Semiconductor Science and Technology*; Bhattacharya, P., Fornari, R., Kamimura, H., Eds.; Elsevier Science: 2011; pp 132−294.

(13) Torricelli, F.; et al. Electrolyte-gated transistors for enhanced performance bioelectronics. *Nature Reviews Methods Primers* **2021**, *1*, 66.

(14) *Light, Water, Hydrogen: The Solar Generation of Hydrogen by Water Photoelectrolysis*, 3rd ed.; Grimes, C. A., Varghese, O. K., Ranjan, S., Eds.; Springer: New York, 2008; pp 115−178.

(15) Nguyen, P.; Teutsch, N.; Wilson, N.; Kahn, J.; Xia, X.; Graham, A.; Kandyba, V.; Giampietri, A.; Barinov, A.; Constantinescu, G.; Yeung, N.; Hine, N.; Xu, X.; Cobden, D.; Wilson, N. Visualizing electrostatic gating effects in two-dimensional heterostructures. *Nature* **2019**, *572*, 220.

(16) Bashirpour, M. Review on Graphene FET and its Application in Biosensing. *International Journal of Bio-Inorganic Hybrid Nanomaterials* **2015**, *4*, 5−13.

(17) Yung, K.; Wu, W.; Pierpoint, M.; Kusmartsev, F. Introduction to graphene electronics − a new era of digital transistors and devices. *Contemporary Physics* **2013**, *54*, 233−251.

(18) Mak, K. F.; Lee, C.; Hone, J.; Shan, J.; Heinz, T. F. Atomically Thin MoS₂: A New Direct-Gap Semiconductor. *Phys. Rev. Lett.* **2010**, *105*, 136805.

(19) Kam, K. K.; Parkinson, B. A. Detailed Photocurrent Spectroscopy of the Semiconducting Group VI Transition Metal Dichalcogenides. *J. Phys. Chem.* **1982**, *86*, 463−467.

(20) *Gmelin Handbook of Inorganic and Organometallic Chemistry*, 8th ed.; Springer-Verlag: Berlin, 1995; Vol. *B7*, pp 1−124.

(21) Yu, Y.; Zhang, K.; Parks, H.; Babar, M.; Carr, S.; Craig, I. M.; Winkle, M. V.; Lyssenko, A.; Taniguchi, T.; Watanabe, K.; Viswanathan, V.; Bediako, D. K. Tunable angle-dependent electrochemistry at twisted bilayer graphene with moiré flat bands. *Nat. Chem.* **2022**, *14*, 267−273.

(22) He, Y.; et al. Self-gating in semiconductor electrocatalysis. *Nat. Mater.* **2019**, *18*, 1098−1104.

(23) Wang, Y.; Kim, C.-H.; Yoo, Y.; Johns, J. E.; Frisbie, C. D. Field Effect Modulation of Heterogeneous Charge Transfer Kinetics at Back-Gated Two-Dimensional *MoS₂* Electrodes. *Nano Lett.* **2017**, *17*, 7586−7592.

(24) Kim, C.-H.; Wang, Y.; Frisbie, C. D. Continuous and Reversible Tuning of Electrochemical Reaction Kinetics on Back-Gated 2D Semiconductor Electrodes: Steady-State Analysis Using a Hydrodynamic Method. *Anal. Chem.* **2019**, *91*, 1627−1635.

(25) Liu, X.; Li, B.; Li, X.; Harutyunyan, A. R.; Hone, J.; Esposito, D. V. The Critical Role of Electrolyte Gating on the Hydrogen Evolution Performance of Monolayer MoS2. *Nano Lett.* **2019**, *19*, 8118−8124.

(26) Ebejer, N.; Güell, A. G.; Lai, S. C.; McKelvey, K.; Snowden, M. E.; Unwin, P. R. Scanning Electrochemical Cell Microscopy: A Versatile Technique for Nanoscale Electrochemistry and Functional Imaging. *Annual Review of Analytical Chemistry* **2013**, *6*, 329−351.

(27) Aaronson, B. D. B.; Chen, C.-H.; Li, H.; Koper, M. T. M.; Lai, S. C. S.; Unwin, P. R. Pseudo-Single-Crystal Electrochemistry on Polycrystalline Electrodes: Visualizing Activity at Grains and Grain Boundaries on Platinum for the Fe2+/Fe3+ Redox Reaction. *J. Am. Chem. Soc.* **2013**, *135*, 3873−3880.

(28) Novoselov, K. S.; Geim, A. K.; Morozov, S. V.; Jiang, D.; Zhang, Y.; Dubonos, S. V.; Grigorieva, I. V.; Firsov, A. A. Electric Field Effect in Atomically Thin Carbon Films. *Science* **2004**, *306*, 666−669.

(29) Novoselov, K. S.; Jiang, D.; Schedin, F.; Booth, T. J.; Khotkevich, V. V.; Morozov, S. V.; Geim, A. K. Two-dimensional atomic crystals. *Proceedings of the National Academy of Sciences* **2005**, *102*, 10451−10453.

(30) Li, H.; Wu, J.; Huang, X.; Lu, G.; Yang, J.; Lu, X.; Xiong, Q.; Zhang, H. Rapid and Reliable Thickness Identification of Two-Dimensional Nanosheets Using Optical Microscopy. *ACS Nano* **2013**, *7* (11), 10344−10353.

(31) Zhang, H.; Ma, Y.; Wan, Y.; Rong, X.; Xie, Z.; Wang, W.; Dai, L. Measuring the Refractive Index of Highly Crystalline Monolayer MoS2 with High Confidence. *Sci. Rep.* **2015**, *5*, 8440.

(32) Splendiani, A.; Sun, L.; Zhang, Y.; Li, T.; Kim, J.; Chim, C. Y.; Galli, G.; Wang, F. Emerging Photoluminescence in Monolayer MoS2. *Nano Lett.* **2010**, *10*, 1271−5.

(33) Mccreary, K.; Hanbicki, A.; Sivaram, S.; Jonker, B. A- and B-Exciton Photoluminescence Intensity Ratio as a Measure of Sample Quality for Transition Metal Dichalcogenide Monolayers. *APL Materials* **2018**, *6*, 111106.

(34) Wang, L.; Meric, I.; Huang, P. Y.; Gao, Q.; Gao, Y.; Tran, H.; Taniguchi, T.; Watanabe, K.; Campos, L. M.; Muller, D. A.; Guo, J.; Kim, P.; Hone, J.; Shepard, K. L.; Dean, C. R. One-Dimensional Electrical Contact to a Two-Dimensional Material. *Science* **2013**, *342*, 614−617.

(35) Edelberg, D.; et al. Approaching the Intrinsic Limit in Transition Metal Diselenides via Point Defect Control. *Nano Lett.* **2019**, *19*, 4371−4379.

(36) *COMSOL Multiphysics Electrochemistry Module Users Guide*, version 5.3; COMSOL: Stockholm, 2017.